CONFINEMENT AND PROFILE CHANGES INDUCED BY THE PRESENCE OF POSITIVE OR NEGATIVE RADIAL ELECTRIC FIELDS IN THE EDGE OF THE TEXTOR TOKAMAK

R.R. WEYNANTS[1], G. VAN OOST[1], G. BERTSCHINGER[2], J. BOEDO[3], P. BRYS[1], T. DELVIGNE[1], K.H. DIPPEL[2], F. DURODIÉ[1], H. EURINGER[2], K.H. FINKEN[2], D.S. GRAY[3], J.D. HEY[2], D.L. HILLIS[4], J.T. HOGAN[4], L. KÖNEN[2], R. LENERS[1], A.M. MESSIAEN[1], A. POSPIESZCZYCK[2], U. SAMM[2], R.P. SCHORN[2], B. SCHWEER[2], G. TELESCA[1], R. VAN NIEUWENHOVE[1], P.E. VANDENPLAS[1]

[1] Laboratoire de physique des plasmas — Laboratorium voor Plasmafysica, Association Euratom-Etat Belge — Associatie Euratom-Belgische Staat, Ecole royale militaire — Koninklijke Militaire School, Brussels, Belgium

[2] Institut für Plasmaphysik, Forschungszentrum Jülich GmbH, Association Euratom-KFA, Jülich, Germany

[3] Institute for Plasma and Fusion Research, University of California at Los Angeles, Los Angeles, California, United States of America

[4] Fusion Energy Division, Oak Ridge National Laboratory, Oak Ridge, Tennessee, United States of America

ABSTRACT. Edge radial electric fields were induced in the edge of the TEXTOR tokamak by means of a polarization electrode in order to study their influence on the plasma edge profiles and its confinement. The studies include the generation of H-mode behaviour with either positive or negative polarity. Particle confinement (τ_p) of deuterium and of impurity ions as well as energy confinement (τ_E) are investigated. For positive fields which remain below the threshold for the L-H transition, an interesting regime of reduced particle confinement without noticeable energy confinement loss is found. A strong asymmetry in the edge density profiles with respect to the electric field sign is observed at these low polarization voltages. Above the threshold, H-mode behaviour with increased energy confinement and especially particle confinement can be produced with either polarity of the applied electric field. It is, however, found that, whereas the energy confinement in positive H-modes is at least as good as that in negative ones, the ratio τ_p/τ_E is about three times lower in the former case.

1. INTRODUCTION

The achievement of H-mode conditions [1] is thought to be of paramount importance for the operation of a fusion reactor. This regime of improved energy confinement also leads quite often to an even larger improvement in particle confinement [2, 3]. The dilution of the fuel and the possible extinction of the burn by impurities, especially the reaction product helium, are sources of great concern [4]. Therefore, it is important to further the understanding of the conditions leading to H-mode behaviour and of the coupling between energy confinement and particle confinement.

Earlier work [5–7] has shown that H-mode behaviour can be achieved in a tokamak in a controlled way by inducing radial electric fields in the plasma edge using electrodes. Sudden plasma readjustments can be triggered which display the features that characterize L-H transitions: density rise, profile steepening and drop in D_α emission. Concomitantly, improvements in both energy confinement and particle confinement are observed. In TEXTOR [6, 7] it was shown that H-modes can be set up irrespective of whether the radial electric field E_r points outwards or inwards. The latter situation will henceforth be called negative H-mode (or H_- mode) and the former positive H-mode (H_+ mode), corresponding

to their respective signs of the edge E_r. It should be recalled that the traditional H-mode [1], which develops 'spontaneously' in many devices, is of the H_- type [8]. The establishment of the transport barrier, assumed to be responsible for confinement improvement, is usually thought to result from the increased shear in the poloidal rotation or in the electric field [9–11].

In the course of these investigations, it became clear that there are differences in the confinement properties of the H_+ and H_- modes [7]. We therefore undertook a systematic study in which the electric field was gradually changed from one polarity to the other in ohmically heated or neutral beam injection (NBI) heated plasmas. Central in this study is the documentation of the ensuing profile modifications and the changes in particle and energy confinement. The investigation of particle confinement deals with three different ion species (deuterium, helium and neon), and no significant differences between them are observed. At edge fields which remain below the threshold for the L–H transition, a strong asymmetry is found with respect to the sign of the field, revealing for positive fields an interesting regime of strongly reduced particle confinement without noticeable loss of energy confinement. When the H-mode is reached above the threshold, both the particle and energy confinement times (τ_p and τ_E) increase with either polarity. The particle confinement in the H_- mode, however, appears to be substantially higher than that in the H_+ mode although the shear of the electric field is comparable in both cases. In contrast, the energy confinement in positive H-modes is similar and is even somewhat higher than in negative ones.

The obvious limitation on the heat load that the electrode can endure imposes an operational limit on the input power, i.e. a relatively low plasma current ($I_p < 200$ kA) and a low neutral beam power ($P_{NI} < 250$ kW). Reciprocating probes are quite useful for describing critical edge parameters such as the electric field and the electron temperature; however, their application is also restricted to relatively low power discharges. For these reasons, the number of discharges with NBI is limited so that most of the data pertain to edge polarization in Ohmic discharges. Nevertheless, NBI (always co-injection) plays a key role, since it facilitates the attainment of the otherwise marginally accessible Ohmic H_- mode [7] and is also used to measure helium concentrations in the plasma centre. The available NBI data further corroborate the differences found in Ohmic discharges between the H_+ mode and the H_- mode.

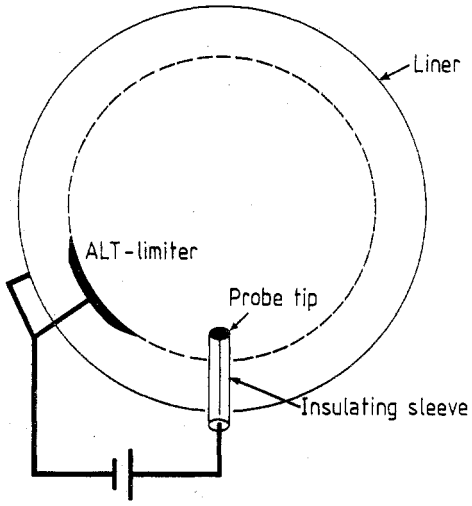

FIG. 1. Schematic drawing of the polarization set-up.

The present paper describes our findings and is organized as follows. In Section 2, the experimental set-up and the operational conditions are described. Section 3 discusses the changes of the electron density n_e, the electron temperature T_e and the radial electric field E_r in the scrape-off layer (SOL) as well as in the high electric field zone inside the limiter radius as a function of the applied electrode voltage. A significant asymmetry with respect to the field sign is observed in the density behaviour. Section 4 deals with the particle confinement of injected trace impurities (Ne, He) and of deuterium. The energy confinement modifications that accompany the electric field variations are described in Section 5, and final conclusions are presented in Section 6. Since most results pertain to the decay rate of the injected impurities (τ_p^*), an interpretative model is presented in Appendix A which allows one to draw conclusions on the confinement time τ_p itself. In Appendix B, the variations in fuelling and exhaust efficiency that result from the observed SOL modifications are studied, since they are used as input for the interpretative model.

Some aspects of this work have been published in abbreviated form in Ref. [12].

2. EXPERIMENTAL SET-UP AND OPERATIONAL CONDITIONS

The set-up used for edge polarization is schematically shown in Fig. 1. The electrode consists of a canoe shaped carbon head, having a length of 13 cm, a width of 3.5 cm and a height of 1.5 cm, mounted on a steel shaft housed in an insulating sleeve made of boron nitride. The electrode is inserted in the plasma, with its longest side aligned with the toroidal direction. A bias

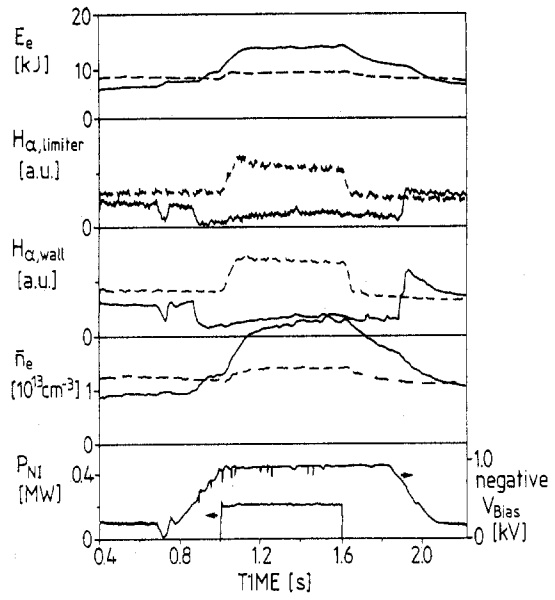

FIG. 2. Time evolution of electron energy, H_α emission at limiter and wall, line density, neutral beam power and polarization voltage without (broken lines) and with (full lines) negative polarization. The neutral beam is present in both cases.

voltage is applied between the electrode and all eight blades of the pumped toroidal belt limiter ALT-II, i.e. the current follows the path: power supply, electrode, plasma, ALT-II, power supply. It is experimentally found that the electrode current I_E is equally distributed over all blades. In the experiments reported here, the probe tip is situated at a plasma radius of 40 cm, i.e. at a distance L = 6 cm inside the limiter radius. The plasma characteristics in the reported experiments are B_t = 2.35 T, I_p = 190 kA, R = 1.75 m, a = 0.46 m, $\bar{n}_e$ = (1-2) × 10^{13} cm^{-3}, T_{e0} = 1-1.5 keV. The applied electrode voltage V_E ranges from -900 V to +900 V, and the absorbed neutral beam power $P_{NI,abs}$ ranges from 110 to 155 kW.

The phenomena connected with the polarization induced effects are illustrated in Fig. 2. The broken lines show the time evolution for an NBI discharge ($P_{NI,abs}$ = 155 kW, t = 1.0-1.6 s) of the line density $\bar{n}_e$, the H_α emission at the limiter and the wall, and the thermal energy in the electron component E_e, obtained by integrating the density and temperature profiles. The beam phase confinement has L-mode character, with the electron confinement time $\tau_{E,e}$ decreasing with respect to the Ohmic phase from 41 ms to 27 ms and the particle confinement time τ_p dropping in about the same proportion. When a -900 V electrode bias is superimposed, a clear H-mode develops (already during the Ohmic phase), yielding a significant gain in density and energy (full lines), with $\tau_{E,e}$ now reaching 33 ms during the beam phase. The relative change in τ_p is much stronger and reaches a factor of about six. Note that before and after the NBI pulse the Ohmic discharge is also in the H-mode during polarization. Earlier descriptions of the effects of the polarization on the main plasma parameters can be found in Refs [6, 7, 12].

We now turn to the systematic description of the plasma response as a function of the applied voltage. All investigations discussed below (documented in Figs 3-21) start from the same standard Ohmic discharge at $\bar{n}_e$ = 0.9 × 10^{13} cm^{-3} to which NBI heating, polarization and trace impurity injection or a combination of these is applied.

Figure 3 shows the electrode current I_E as a function of V_E. The closed symbols pertain to positive or negative H-mode conditions. In this and all later figures (unless specifically stated otherwise) the lines are only fits through the experimental data points pertaining to the Ohmic conditions. The dynamics of the H-mode transition in relation to the electrode parameters have been described in Ref. [13], where it was shown that the jumps in I_E correspond to discontinuous changes in the electric field (see also Fig. 5) and are a manifestation of abruptly reduced poloidal damping and accelerated rotation [13, 14]. The H-mode can only be reached when a minimal probe current [7] is drawn (but not sustained); under our experimental conditions it reaches about 130 ± 20 A for positive V_E, corresponding to a current density of about 4 A/cm^2. To draw this current, a minimum voltage has to be applied. This threshold value depends on the wall conditions and lies between 400 V and 500 V for boronized TEXTOR walls and

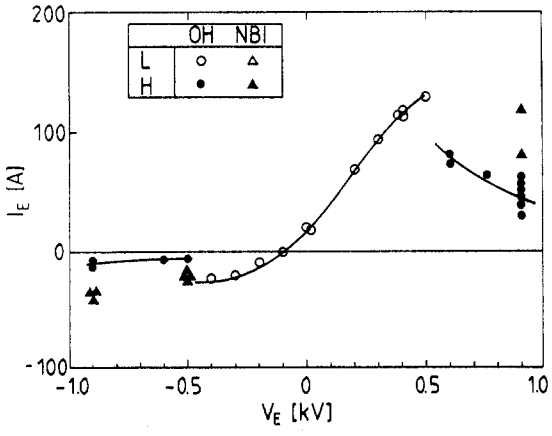

FIG. 3. Variation of the electrode current I_E with electrode voltage V_E for different conditions identified in the inset. The lines are fits through the experimental data points obtained without beams.

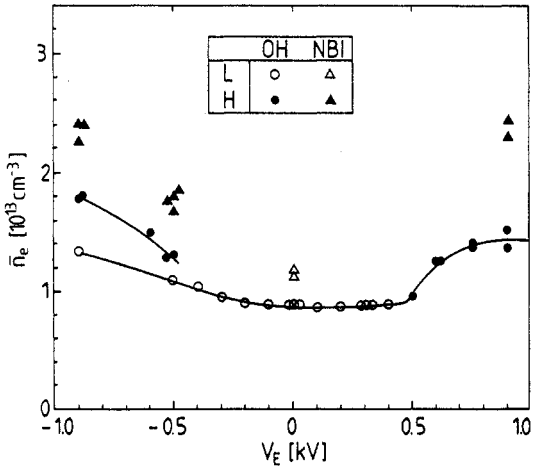

FIG. 4. Variation of the line density $\bar{n}_e$ with electrode voltage V_E. The fuelling gas feedback is set to provide a constant density of $\bar{n}_e = 0.9 \times 10^{13}$ cm^{-3}.

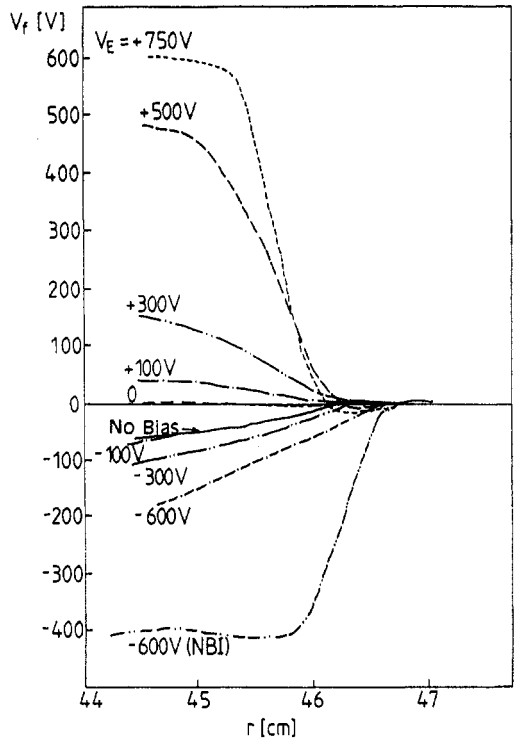

FIG. 5. Radial profile of the floating potential V_f in the plasma edge for representative polarization conditions. The electrode is located between r = 40 cm and r = 41.5 cm. The radial resolution of the Langmuir probe is 1 mm.

positive polarization. With carbonized walls the threshold is typically 100 V higher. At negative electrode voltages, only intermittent H-mode behaviour could hitherto be established in pure Ohmic discharges, suggesting that the electrode current (= ion saturation current) just marginally reaches the minimal Ohmic transition current. This suggests that the latter is of the order of 30–40 A, i.e. appreciably lower than the 130 A observed in the case of positive voltage. The access to the H_ mode is facilitated in NBI heated plasmas, and pure Ohmic H_ modes can be sustained after NBI switch-off. In the CCT tokamak [5, 13], Ohmic H_ modes were readily obtained using emissive electrodes, capable of much higher negative currents, and a similar asymmetry in I_E with respect to the sign of V_E was observed. A possible explanation of this is that the inherent ion orbit loss from the plasma [14] is of the order of 45 A and that it counteracts the action of the electrode current with positive bias and re-enforces it with negative bias.

Figure 4 shows the observed variation of $\bar{n}_e$ with applied voltage. Density increases characterize all H-mode cases, whereas no density change occurs in the range -200 V to 400 V. The density feedback is set to provide a constant density of 0.9×10^{13} cm^{-3}. It is interesting to note that additional gas fuelling is only necessary during the biasing time interval for the voltages $0 < V_E < +500$ V in Ohmic discharges and that the valve remains closed for all other conditions.

3. PROFILES

3.1. Electric field

Figure 5 shows the profiles of the floating potential V_f in the plasma edge, measured by Langmuir probes under a number of experimental conditions. Since the electron temperature changes only weakly over the radial range of the measurement (see Fig. 10), the derivative of these profiles is very nearly the same as that for the plasma potential and quite accurately yields the radial electric field.

The unbiased Ohmic plasma is negatively charged and sustains a gradient of -50 V/cm. A gradual potential increase is observed with positive bias. However, upon the L–H transition the electric field increases abruptly, on a time-scale of about 1.2 ms, by a factor of three (e.g. from +150 V/cm to +450 V/cm for positive bias). In the H-mode, a very strong localization of the field occurs, yielding values of up to ±1000 V/cm, with a full width at half maximum of less than 0.5 cm.

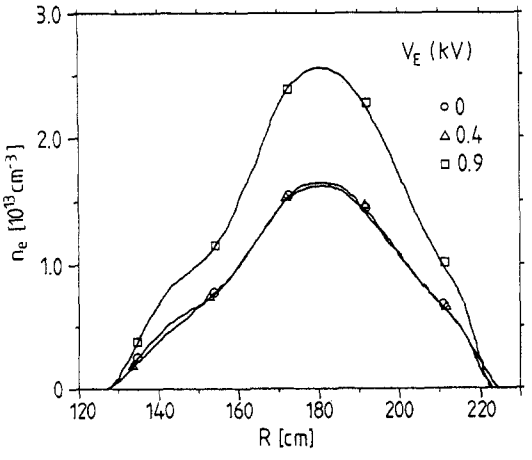

FIG. 6. Interferometric density profiles for V_E = 0, +400 V and +900 V (Ohmic conditions).

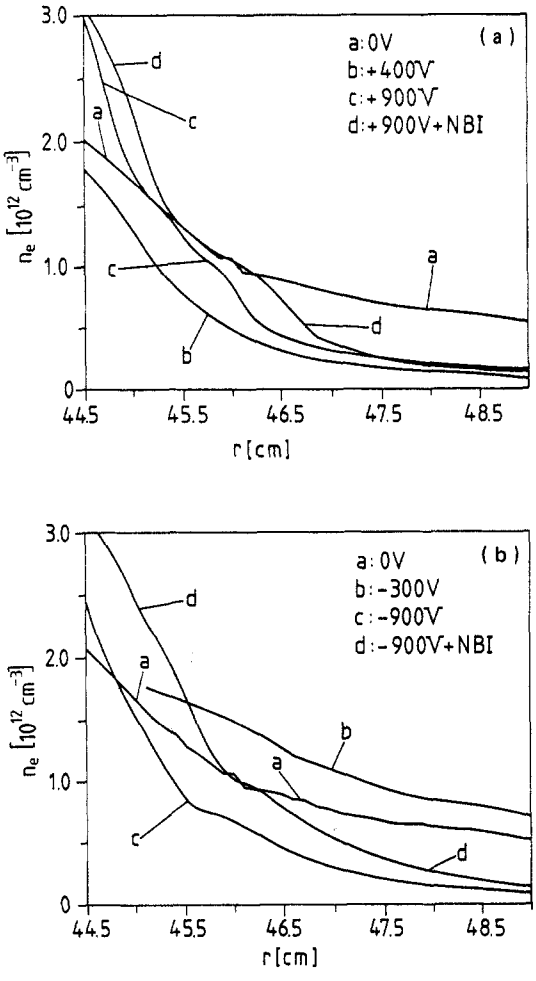

FIG. 7. Radial profiles of density obtained by lithium beam spectroscopy for representative conditions: (a) with positive bias and (b) with negative bias.

Although the electrode is located between r = 40 cm and r = 41.5 cm, the field is appreciable only in the immediate vicinity of the limiter. In Ref. [7] we reported fields which were, for the same applied voltage, only one third as high and which peaked deeper in the plasma. Both of these changes and the already mentioned decrease in the voltage threshold occurred when boronized walls were used instead of carbonized walls. Figure 5 shows that it is difficult to increase the fields with negative bias. However, since the Ohmic plasma has already a negative field, the absolute values of the fields at equal magnitude of the applied voltage are quite similar. There is no significant difference in field strength or field shear between H_+ and H_- modes. The total field structure is displaced (as can also be seen for the density profiles in Fig. 7) to even larger radii by the addition of NBI, as shown in Fig. 5.

3.2. Density

The bulk density profile does not show significant changes unless the voltage is above the transition

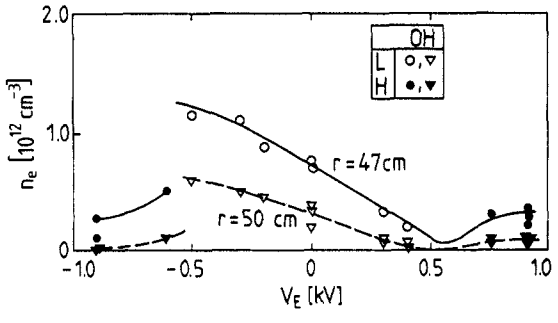

FIG. 8. Variation of the electron density n_e with electrode voltage V_E in the SOL at r = 47 cm and r = 50 cm (only Ohmic conditions).

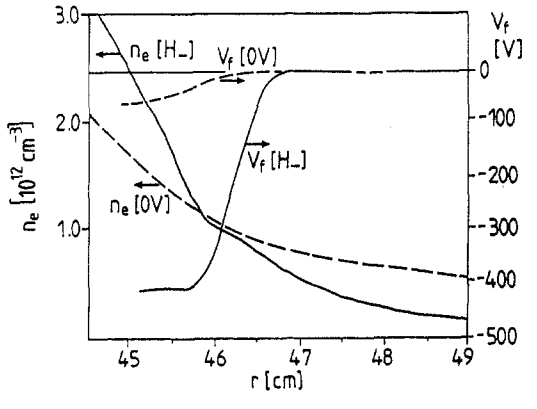

FIG. 9. Radial profiles of density and floating potential for V_E = 0 (Ohmic) and V_E = -600 V (NBI heated H_- mode).

threshold. Figure 6 shows the interferometric profiles in ohmically heated plasmas with V_E = 0 V, +400 V and +900 V. Only directly in the edge of the plasma are there differences between the first two voltages; these differences were further investigated by lithium beam spectroscopy (LBS) and Langmuir double probe measurements. Figure 7(a) shows edge profiles obtained by LBS for representative positive voltages. Results for negative V_E are shown in Fig. 7(b). A strong asymmetry exists between positive and negative bias, at least below the threshold, as can be seen by comparing the curves labelled b in both figures. Further documentation is given in Fig. 8, where the variation with V_E of the density at r = 47 cm and r = 50 cm is plotted for Ohmic discharges. Positive bias provokes a strong reduction in SOL density with respect to the unbiased case; with negative bias the density actually increases. This asymmetry might also have some bearing on the differences in the electric field: the higher the density, the stronger the poloidal viscosity and the weaker the rotation and the electric field [13, 14].

Once the transition occurs, there is no significant difference between the two polarities. The characteristic feature of transition is the edge steepening of the density profile (curves c and d in Fig. 7) which continues in the bulk (Fig. 6). This steepening is correlated with a steepening of the V_f profile and could be imagined as a pivoting around the radial zone where the electric field is highest (see Fig. 9). Furthermore, a local flattening may be present at this very location; this flattening is usually shown by the probes to be even stronger [12]. As already mentioned for the electric field, the beams also tend to shift the density profile outward while maintaining the local flattening.

3.3. Electron temperature

Electron temperature profiles were measured with double Langmuir probes. In contrast to the edge density, the edge electron temperature around the limiter radius does not show asymmetries or strong gradients (see Fig. 10). After the transition, however, a local peak forms in the high field region where also the density flattening is observed (see Section 3.2). Without wanting to digress too much from the subject of the present paper, we have to recall the observation reported in Ref. [12] that in the few discharges for which also fluctuation measurements (all positive H-mode cases) are available, a strong local enhancement of an instability is seen in the high field region. Our present database does not allow us to establish the causality between these different features, for example whether this instability is an essential feature of the transition or whether the threshold for the instability fortuitously coincides with the transition threshold.

Figure 11 shows the bulk T_e profiles from ECE corresponding to the density profiles of Fig. 6. No significant changes are seen, except for a local depression around r = 35 cm in the H-mode cases. This feature develops on a time-scale of 100 ms and is due to increased radiation around this radius which results mainly from the strong local density increase and a minor increase in Z_{eff}. This temperature decrease can be particularly strong for the H_- mode.

3.4. Discussion of the physics

The electric field profile is of particular importance, as its shear is thought to affect confinement [9–11]. It

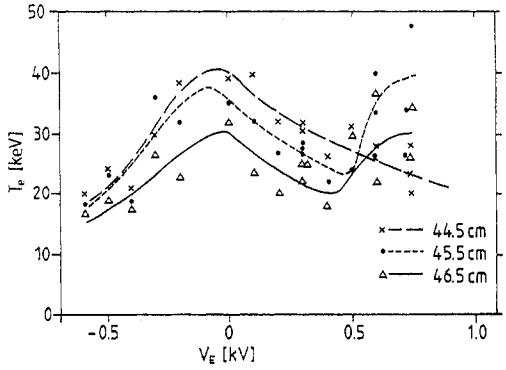

FIG. 10. Variation of the electron temperature T_e with electrode voltage V_E. T_e was obtained by Langmuir probe measurements in the SOL at r = 44.5, 45.5 and 46.5 cm (only Ohmic conditions).

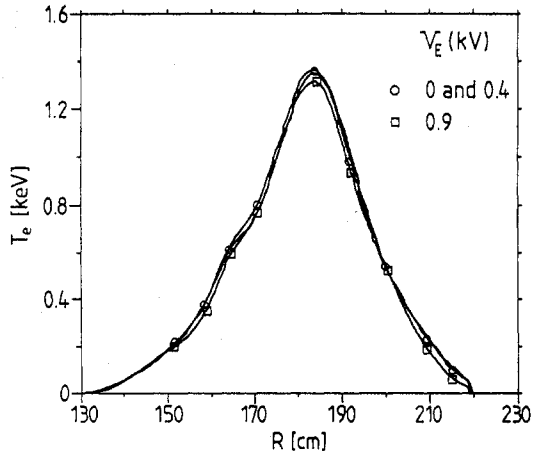

FIG. 11. Electron temperature profiles in the bulk plasma for the conditions of Fig. 6. The profiles at V_E = 0 and 400 V are indistinguishable.

is therefore appropriate to discuss the physics that is involved in shaping the profiles in these experiments.

In general, the radial dependence of E_r is determined by the orthogonal conductivity equation $j_r = \sigma_r E_r$ [13], where σ_r is the radial conductivity. The field scale length can then be imposed by j_r and σ_r or a combination of these. Because of the deep penetration of the electrode into the plasma, the current density drawn by the electrode is constant over 5 cm (except for a negligible 1/r dependence). As argued in Section 2, the inherent thermal ion losses [14] constitute only a fraction of the total j_r and are therefore not capable of enforcing their scale length, which is the poloidal ion Larmor radius. Under our experimental conditions the latter is typically 1.2–1.4 cm. The experimentally found strong localization of E_r in the very edge of the plasma might therefore result only from the σ_r profile effect. As stated in Ref. [13], the theoretical description of the orthogonal conductivity requires further scrutiny. One expects a neoclassical contribution which, if it is mainly due to ion–ion collisions [13], yields $\sigma_r = m_i n_e \nu_{ii} f(E_r) q^2/B_t^2$, where ν_{ii} is the ion–ion collision frequency. The average collisionality ν_{ii}^* under our conditions is about 7 ± 4. The factor $f(E_r)$ makes σ_r become non-linear above the L–H threshold. The main radial dependence is nevertheless thought to come from $n_e \nu_{ii}$ (i.e. mainly n_e^2) such that σ_r decreases (and E_r increases) strongly with increasing radius. Ion–neutral collisions should be particularly strong in the limiter zone (as also sugegsted by the experimentally found dependence on wall conditioning) and should yield $\sigma_r = 2 m_i n_e n_0 \langle \sigma_{cx} v \rangle q^2/B_t^2$, where n_0 is the neutral density and $\langle \sigma_{cx} v \rangle$ is the charge exchange rate coefficient. Therefore, at the very edge of the plasma, an increase of σ_r (and a decrease of E_r) should occur because of the expected exponential increase of the neutral density.

The electron density profile clearly steepens in the plasma edge, but no equivalent feature is seen for the temperature profile, implying the formation of a particle transport barrier only. Since the bulk T_e profiles for 0 V and 900 V in Fig. 11 are nearly identical, the increased confinement in the H-mode (see Section 5) could be linked with an electron thermal conductivity χ_e which scales as $1/n_e$, and with a density rise resulting from the particle barrier.

4. PARTICLE CONFINEMENT

Particle confinement can most easily be studied by injecting trace elements into the plasma and observing their exhaust rates. Such techniques were applied, using helium and neon. Since TEXTOR is equipped with a pump limiter, valuable information can be gained from the rate at which these impurities can be pumped (including helium, since turbomolecular pumps are used). The confinement of the main ion plasma component deuterium was derived by balancing the loss rate with the ionization rate inferred from D_α emission measurements. The latter procedure is more difficult, since it relies on a correct evaluation of all the possible sources and their spatial distribution. We start our presentation with the results on injected impurities. Care has been taken to ensure that the injected impurities remain trace elements, i.e. they do not affect the macroscopic plasma parameters. A more detailed account of the helium results will be given in a forthcoming paper [15].

4.1. Neon confinement

An identical, short (100 ms) neon puff was injected at t = 1.1 s into plasmas where a constant bias prevailed for 1 s, starting at t = 0.9 s. The bulk neon was moni-

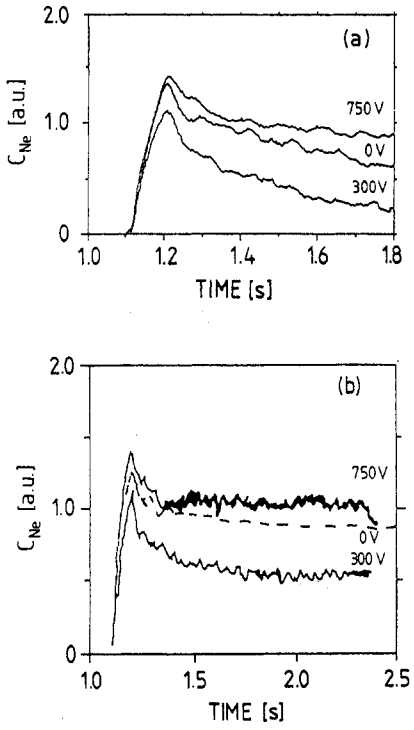

FIG. 12. Time decay of the neon concentration C_{Ne} following a neon puff between t = 1.1 and 1.2 s, with (a) and without (b) ALT-II pumping. A constant polarization pulse is applied from t = 0.9 s to t = 1.9 s in case (a) and to t = 2.4 s in case (b).

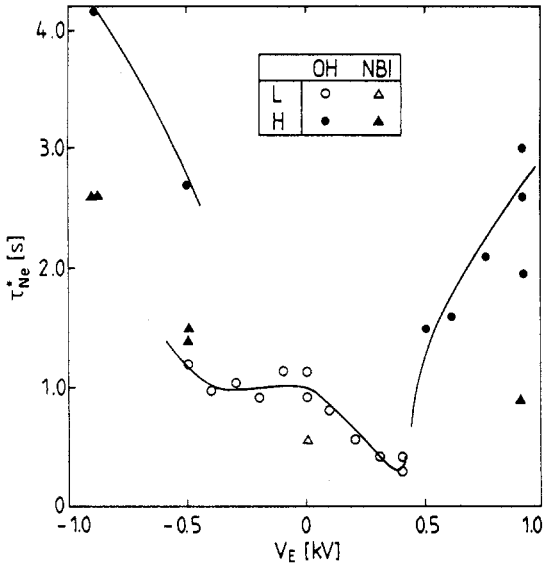

FIG. 13. Variation of the neon decay time τ^*_{Ne} with electrode voltage V_E for different conditions identified in the inset.

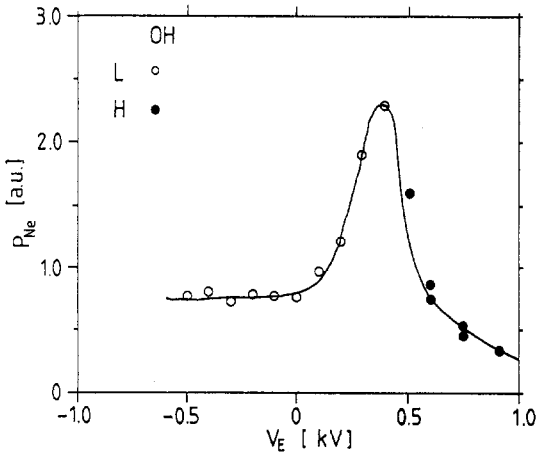

FIG. 14. Variation of the partial neon pressure P_{Ne} versus the electrode voltage V_E. The neon pressure is measured in the pumping duct of ALT-II for Ohmic polarization conditions.

tored using a Ne VIII line at 770.4 Å. The Ne VIII brilliance is proportional to the local electron density, the Ne^{7+} concentration (C_{Ne}) and the excitation rate $X(T_e)$ in a shell around r = 25 cm. C_{Ne} is simply taken as the ratio of the measured brilliance to the electron line density. This is fully warranted for all Ohmic discharges, where the electron temperature profile remains constant over the full experimental range and the overall shape of the density profile is preserved (see Fig. 11). Comparing Ohmic cases with beam heated cases, this ratio is only a first, yet reasonable, approximation for the C_{Ne} changes: the temperature profiles change weakly because of the extra density rise and the poor L-mode confinement of these discharges. The neon flux at the limiter was measured using a Ne I line at 6402 Å and the neon neutral pressure in the pumping duct of ALT-II monitored with a residual gas analyser (mass 20 or 22).

The time decay of C_{Ne} for discharges at V_E = 0, 300 and 750 V is shown in Fig. 12(a) for full ALT-II pumping and in Fig. 12(b) without pumping. In both cases there is a relatively fast decay, followed by a stationary level in Fig. 12(b) and a further decay (at a much slower pace) in Fig. 12(a). This latter decay is the result of pumping. Since the decay is quite exponential, an effective confinement time τ^*_p (denoted τ^*_{Ne}) can be defined. Figure 13 shows this quantity as a function of V_E for the different experimental conditions. The extremely long decay times in the Ohmic H_- mode precludes an accurate measurement in the experimentally available time span ($\tau^*_{Ne} > 4$ s). A pronounced dependence on the polarity is found both in the pre-transition phase and the post-transition phase, with τ^*_{Ne} being systematically lower for positive E_r. The cases with beam heating show under all conditions lower confinement and uphold the polarity dependence. At V_E = +300 to +400 V, extremely short decay times are found.

The neon pressure measured in the pumping ducts of ALT-II changes inversely to τ^*_{Ne}, as seen in Fig. 14. A strongly enhanced exhaust around +400 V and a drastic reduction, even with respect to the unbiased condition, is exhibited in the H-mode.

4.2. Helium confinement

A 10 ms helium puff was injected at t = 0.6 s. The polarization voltage was ramped up from 0.7 s to 1.0 s, then kept constant up to 1.8 s and finally ramped down to 2.1 s; NBI was applied from 1.3 s to 1.8 s. The core helium density is measured by charge exchange excitation (CXE) spectroscopy. The 4686 Å line emission of He^+ is observed along a line of sight intersecting the neutral beam. The observed photon flux can yield the local density of the He^{2+} ions that were instrumental in creating the He^+ through charge exchange with the beam neutrals. The helium neutral pressure in the pumping duct of ALT-II was measured from the helium light emerging from a modified Penning gas discharge [16].

Since the neutral beam is a prerequisite for the core measurement, the decay rate experiments concentrated

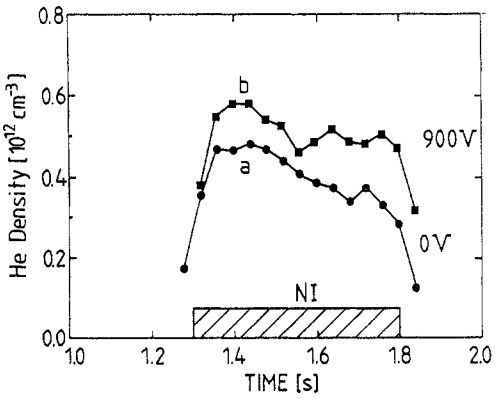

FIG. 15. Time decay of the He^{2+} ions detected by CXE using the injected beam, with and without polarization (r = 25 cm). The polarization voltage is 900 V, lasting from t = 1.0 s to t = 1.8 s. The gas puff lasted from 0.60 s to 0.61 s.

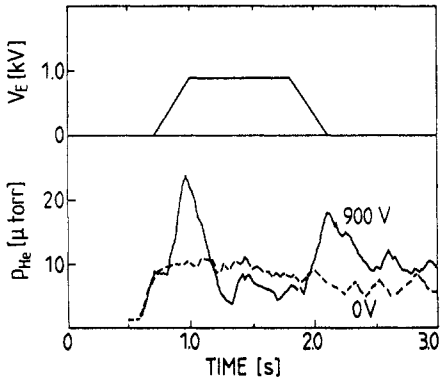

FIG. 16. Time variation of the partial helium pressure measured in the pumping duct of ALT-II for Ohmic conditions without (broken line) and with (+900 V, full line) polarization. The gas puff lasted from 0.60 s to 0.61 s. The pressure monitor has a 0.1 s integration time. The arrows mark the times at which the discharge switches to the H-mode and then reverts from it.

on the difference between beam heated discharges with and without biasing, as shown, for example, in Fig. 15 ($P_{NI,abs}$ = 115 kW). Curve a shows the time behaviour of the He^{2+} ions (at r = 25 cm) in a discharge without bias and curve b shows that in an H_+ discharge at V_E = +900 V. The helium decay time τ^*_{He} is clearly much longer in the H-mode. Typical values for τ^*_{He} are 0.85 ± 0.25 s in the beam heated L-mode discharges and 2.4 ± 1.0 s in the H_+ mode discharges.

Measurements of the partial helium pressure in the duct reveal a behaviour which is quite analogous to that of neon shown in Fig. 14. Whereas the exhaust strongly peaks around +400 V, it drops below the no-bias level after the transition to the H-mode. The effect is shown in Fig. 16 during a beamless discharge in which a trapezoidal polarization voltage was applied. The behaviour found from the steady state discharges as a function of V_E is displayed versus time; a strong exhaust is clearly seen to take place during the ramp-up and ramp-down of the polarization voltage, i.e. every time the voltage range around 350 V is passed. An H-mode phase exists between the times marked by the arrows. It should also be noted that the pressure monitor has an integration time of 0.1 s.

4.3. Deuterium confinement

As explained before, the determination of the deuterium confinement relies on the ionization rates inferred from D_α emission measurements. The main contributions to deuterium recycling come from the limiter ($D_{\alpha,\ell}$), the liner ($D_{\alpha,w}$) and the biasing electrode ($D_{\alpha,e}$). As usual, it is assumed that $D_{\alpha,\ell}$ and $D_{\alpha,w}$ are toroidally symmetric. Only the limiter signal was absolutely calibrated in these experiments. The emission from the electrode can be approximately calibrated in the following way. Upon introducing the unbiased electrode into the plasma, $D_{\alpha,\ell}$ and $D_{\alpha,w}$ both drop to about 0.7 of the level they attain in an electrodeless discharge having the same density. Assuming that the particle confinement is not affected by the mere physical presence of the electrode, we conclude that 30% of

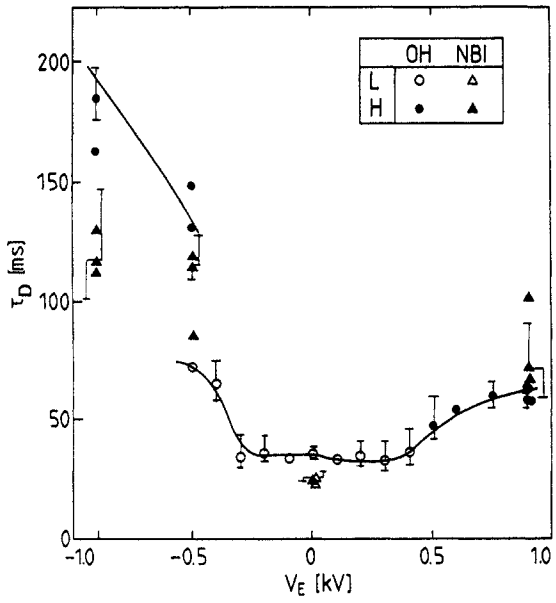

FIG. 17. Variation of the deuterium confinement time τ_D (from D_α emission) with electrode voltage V_E, for different conditions identified in the inset. The error bars reflect possible errors introduced by different weighting of the ionization sources.

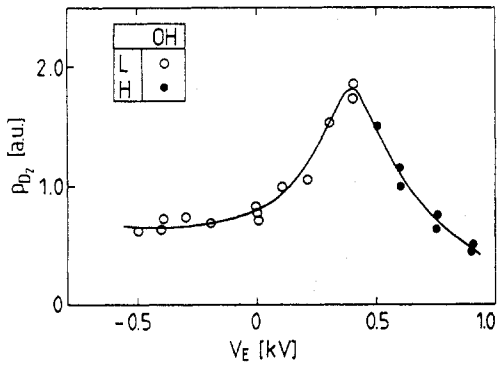

FIG. 18. Variation of the partial deuterium pressure P_{D_2} versus the electrode voltage V_E. The deuterium pressure is measured in the pumping duct of ALT-II for Ohmic polarization conditions.

the recycling is taken over by the electrode. The sharing between limiter and wall is, from earlier experience, assumed to be at a ratio of 4 to 1. The total ionization rate R_i is then found by combining the observed D_α photon fluxes with weighting factors such that in the $V_E = 0$ V Ohmic discharge the recycling flux is shared at a ratio of 0.56/0.3/0.14 by the limiter, the electrode and the wall, respectively. The conversion factor of ionization events to excitation events was assumed to be constant at a value of 14 [17]. The deuterium confinement time τ_D is finally equated to the ratio of the total number of electrons in the discharge to the total ionization rate. The results of this procedure are shown in Fig. 17, where τ_D is plotted versus V_E for the various plasma conditions studied before. The effect of possible errors in the relative weighting factors can be judged from the error bars; the lower ends of the bars correspond to the set of weighting factors (0.4, 0.5, 0.1) and the upper ends to (0.72, 0.1, 0.18).

The variation of τ_D shows several features that were also found for τ^*_{Ne}. The apparent decreased confinement at small positive V_E values is, however, less pronounced. There may be several reasons for this. Inside the voltage range (0, +400 V) an external gas feed is applied, but no direct observation of D_α emission in the injection zone is available. In the same voltage domain the $D_{\alpha,\ell}$ and $D_{\alpha,w}$ signals decrease, whereas $D_{\alpha,e}$ increases strongly; it is possible that a change in their respective weighting factors influences the results. In contrast, for H-mode conditions, all three signals decrease with respect to the no-bias case, and the interpretation is straightforward.

The partial deuterium pressure in the pumping duct was measured by a mass spectrometer (mass 4). The dependence on the probe voltage closely resembles that already found for neon and helium and is shown in Fig. 18.

4.4. Interpretation of results

The decay times τ^*_p and the partial pressures in the pumping duct do not depend in a simple manner on the particle confinement times of the respective ions. In order to derive the latter, a recycling model is presented
in Appendix A which extends an earlier model presented in Ref. [18] by including the effects of pumping.

We introduce the following definitions: N_p is the number of ions of a given species in the discharge at a certain time; N_{tot} is the total number of particles of that species injected until that time; f is the fuelling efficiency; R is the reflection coefficient, i.e. the probability for reflection from the wall (limiter) of an incident particle; τ_w is the effective confinement time of the wall, describing the average dwell time in the wall; and ϵ is the exhaust efficiency defined as the fraction of the plasma efflux that is pumped. The following analytic results can then be obtained from this model (see Appendix A for the approximations involved):

(a) Without pumping, a stationary level of N_p ($N_{p,s}$) is reached after an initial decay (case Fig. 12(b)). This level is given by

$$N_{p,s} = \frac{f\tau_p}{(1 - fR)\tau_w + f\tau_p} N_{tot} \quad (1)$$

(b) With pumping, a further decay occurs at a slower decay rate, τ^*_p, given by

$$\tau^*_p = ((1 - fR)\tau_w + f\tau_p)/f\epsilon \quad (2)$$

(c) The partial pressure measured in the duct is given by

$$p = 4.4 \times 10^{-21} N_{tot}/(\tau^*_p S_{eff}) \quad (3)$$

where S_{eff} is the effective pumping speed for the element considered. A temperature of 300 K in the pump volume is assumed, and SI units are used.

The last two results readily explain the noted complementarity between Fig. 13 and Fig. 14, since the partial pressure must indeed change as the inverse of τ^*_p. Equation (2) shows that the relation between τ^*_p and τ_p is not a simple one, since it involves such diverse and poorly known parameters as τ_w, f, R and ϵ. Whereas τ^*_p is the more relevant quantity when studying plasma exhaust, τ_p is the more interesting characterization of the plasma proper.

It would clearly be of interest to know to what extent the more readily accessible τ^*_p tracks the underlying

TABLE I. VARIATION OF τ_p AS A FUNCTION OF BIAS VOLTAGE FOR NEON

	V_E = 0 V	V_E = 300 V	V_E = 750 V
$N_{p,s}/N_{tot}$	1	0.60	1.17
τ^*_{Ne}	1	0.4	2.1
τ_{Ne}/ϵ	1	0.24	2.5
τ_{Ne}	1	0.17	1.4

changes in τ_p. Combining Eqs (1) and (2), one can *formally* write

$$N_{p,s} = (\tau_p/\epsilon\tau^*_p)\, N_{tot} \quad (4)$$

Provided that ϵ is determined independently, the relative change of τ_p from one experimental condition to another can be obtained by performing for each of these conditions two measurements (Figs 12(a) and 12(b)): one measurement for $N_{p,s}$ without pumping and the other for τ^*_p with pumping. Applying Eq. (4) to the specific cases of Figs 12 yields the results listed in Table I. The values of $N_{p,s}/N_{tot}$ and τ^*_{Ne} (= 1 s) obtained at V_E = 0 V are used for normalization. A first approximation for the variation of ϵ from one condition to the other is defined in Appendix B. These calculations suggest furthermore that decreases in ϵ of about a factor of two can occur under H-mode conditions.

The example of Table I shows that the differences between the two times can be quite high. The trend in the τ_p change is, however, brought out by τ^*_p. This is thought to be certainly the case when τ^*_p for the same species is compared under experimental conditions in which the SOL parameters are similar (i.e. for comparable τ_w, f, R and ϵ), as is the case in H_+ and H_- modes. It is in this spirit that we will use τ_p and τ^*_p exchangeably in our further discussions (see also Table III for the cases in which the values τ_D and τ^*_D were obtained independently).

4.5. Discussion of results

The results on particle confinement and exhaust can be summarized as follows:

(i) An interesting regime of reduced particle confinement was found to exist at positive electric field values (E_r = 100–150 V/cm) below the threshold for transition to the H-mode. Table II compares the particle confinement results at V_E = 350 V with those at V_E = 0 V, which for each case are normalized to unity. The entry τ^*_{p1} gives τ^*_p as derived from the decay measurements, whereas τ^*_{p2} is based on Eq. (3). The reduction in τ^*_p is remarkably similar for the three species considered. As discussed before, the discrepancy between τ_p and τ^*_p for deuterium might be due to the delicate nature of the accounting for the recycling sources in the case of τ_p.

The decrease in particle confinement can possibly be explained as follows. With the application of a positive voltage, the electrode continuously extracts electrons from the plasma. The plasma response consists of the driving out of an equally large current of ions of all species, resulting in a closing of the electrode current path. For negative voltages, electrons are injected and ions are drawn into the plasma. Thus, an asymmetry develops that is accentuated by the very different magnitudes of the respective currents. Note that we are describing here the steady state conditions. There is a transient phase upon polarization switch-on (lasting about a rotation damping time [13]) where the plasma response lags behind and the electrode is able to charge up the plasma, thus setting up the electric field.

(ii) It should be noted that the steady state neon level in Table I only drops by about 1.6 while τ_p decreases by a factor of almost six at V_E = 300 V. Equation (1) shows that in the limit where τ_w is small, the stationary level would be constant and independent of τ_p, whereas in the limit where τ_w is very large, we would have $N_{p,s}/N_{tot} = [f/(1 - fR)]\tau_p/\tau_w$. Also in this second limit the final result can be rather insensitive to a change in τ_p, as the latter can be compensated by an increase in F = f/(1 − fR) and/or a decrease in τ_w.

TABLE II. REDUCTION IN PARTICLE CONFINEMENT (NORMALIZED TO UNBIASED CONDITIONS) FOR POSITIVE EDGE POLARIZATION BELOW THE TRANSITION THRESHOLD IN OHMICALLY HEATED PLASMAS

Species	Parameter	V_E = +350 V
Neon	τ^*_{p1}	0.35
	τ^*_{p2}	0.34
	τ_p	0.2
Helium	τ^*_{p2}	0.38
Deuterium	τ^*_{p2}	0.42
	τ_p	0.9

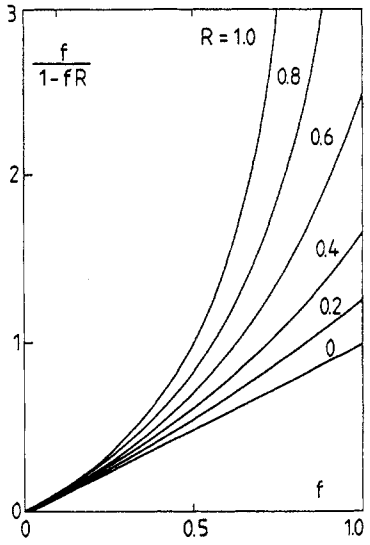

FIG. 19. Variation of $F = f/(1 - fR)$ with the fuelling efficiency f for various values of the reflection coefficient R.

TABLE III. ENHANCEMENT OF PARTICLE CONFINEMENT IN H-MODE PLASMAS (AS COMPARED TO THE UNBIASED CASE)

Species	Discharge	Parameter	H_+ (+900 V)	H_- (-900 V)
Neon	Ohmic	τ^*_{p1}	2.4	>4
		τ^*_{p2}	2.3	—
		τ_p	1.4	—
	Beam	τ^*_{p1}	1.6	4.7
		τ^*_{p2}	1.4	—
Helium	Ohmic	τ^*_{p2}	1.4	—
	Beam	τ^*_{p1}	2.8	—
		τ^*_{p2}	2.0	—
Deuterium	Ohmic	τ_p	1.7	5.3
		τ^*_{p2}	1.5	—
	Beam	τ_p	3.2	4.8
		τ^*_{p2}	1.6	—

Figure 19 shows the variation of F with f for different values of R (typically, R is expected to be 0.5-0.6 [18]). As shown in Appendix B, the SOL profile changes occurring when going from $V_E = 0$ V to $V_E = 300$ V, for neon, are compatible with changes in F by a factor of 2.5.

(iii) Under H-mode conditions the particle confinement always increases strongly. Table III summarizes the observations. The entries are the same as in Table II, but here beam heated discharges ($P_{NI,abs} = 110$–155 kW) are also included. The unbiased conditions are again used for normalization. The confinement of all three species considered increases about equally. The improvement is, broadly speaking, quite similar in the Ohmic and the beam heated discharges. In some cases the enhancement appears larger in the Ohmic discharge, while in other instances the improvement is larger in the beam heated discharge. This is probably an indication of the inevitable errors in these measurements. The H_- modes seem to have substantially higher confinement in both Ohmic and beam heated plasmas.

5. ENERGY CONFINEMENT

The energy confinement characteristics in the H_+ mode have been described earlier [7] and can be summarized as follows. Over the experimental density range the stored energy depends on $\bar{n}_e$ in standard TEXTOR Ohmic and NBI heated plasmas. Since the polarization brings about a positive increment in energy which is roughly density independent, the relative improvement of τ_E is weakest at high density. For an example of the net energy gain at constant density, we refer the reader to Fig. 1(a-c) in Ref. [7]. At $\bar{n}_e = 1.4 \times 10^{13}$ cm^{-3}, typical increases are about 1.2 in Ohmic discharges and 1.3 in beam heated ones.

A typical variation of energy confinement with electrode voltage is given in Fig. 20, which shows the electron energy confinement time $\tau_{E,e}$ obtained from the measured electron density and temperature profiles. Comparison with the diamagnetic and equilibrium energies shows that the electrons contribute about 70% to the

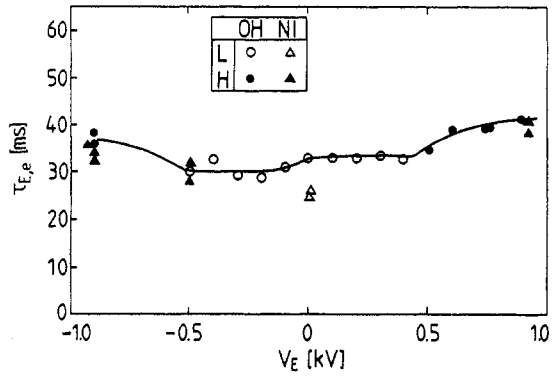

FIG. 20. Electron energy confinement time $\tau_{E,e}$ versus electrode voltage V_E for different conditions identified in the inset.

TABLE IV. ENERGY CONFINEMENT ENHANCEMENT FACTOR (OVER NO-BIAS) IN H-MODE PLASMAS

	Ohmic	Beam heated
H_+ (+900 V)	1.30	1.55
H_- (-900 V)	1.15	1.30

total kinetic energy. We prefer to discuss the confinement in terms of thermal values, since the fast particle contribution included in the diamagnetic or MHD energies obscures the issue for operation with beams. No change in energy confinement is observed when going from 0 V to +400 V, notwithstanding the strong edge and particle confinement changes reported in Sections 3 and 4. The confinement enhancement in the H-mode cases is summarized in Table IV (see Fig. 4 for the pertaining densities). Positive H-modes do not have lower confinement than negative ones. In fact, they appear to be somewhat superior.

The power used to polarize the plasma ($P_E = V_E I_E$) is not taken into account when calculating τ_E. Our justification for this is twofold:

(i) At $V_E = +450$ V (see Fig. 3), P_E constitutes about 60 kW, i.e. a fraction of 0.25 of the Ohmic power P_{OH}, and yet no change whatsoever in plasma energy (or any other parameter inside r = 44 cm) is observed. This is of course to be expected, as P_E is deposited in the outer plasma edge where the local confinement is usually thought to be extremely poor [19]. Thus, not including P_E ensures that the unchanged τ_E reflects the identical energy transport conditions prevailing at $V_E = 0$ V and 450 V, respectively.

(ii) In Ohmic H_+ modes, P_E reaches about 65 kW (i.e. 0.28 of P_{OH}) at $V_E = +500$ V and drops to 40 kW at $V_E = +900$ V (0.17 P_{OH}, less than at $V_E = +500$ V). The energy increment achieved upon transition is clearly not dependent on the electrode power. P_E is typically 0.1 P_{OH} for Ohmic H_- modes. In the beam heated discharges, P_E attains 0.25 ($P_{OH} + P_{NI}$) in H_+ modes and 0.1 ($P_{OH} + P_{NI}$) in H_- modes. When the electrode power is added, the differences between H_+ and H_- tend to disappear.

Inspection of Figs 13, 17, 18 and 20 reveals that the magnitude of the confinement in the H-mode depends on the magnitude of the edge field, although the energy confinement might saturate somewhat faster than the particle confinement. Since part of the energy increase is due to the density increase, the gains in energy and particle confinement are linked, and more experiments are needed to assess the finer details. The magnitude of the electric field might be thought to impose a natural gradation in the H-mode condition and this fact should perhaps be borne in mind when comparing results obtained on different machines.

6. DISCUSSION AND CONCLUSIONS

The first part of this study described the changes, as a function of the imposed electrode potential, in the edge profiles of important parameters. Of particular interest is the electric field profile. The scale length of E_r is in principle imposed by the scale lengths of the current density j_r and the radial conductivity σ_r or a combination of both. Since j_r in our experiments is essentially constant over the outer 5 cm of the plasma, only σ_r is capable of tailoring E_r. In other experiments where j_r is mainly constituted by the ion losses, an additional constraint is introduced. Our experiments show, however, that even under the latter conditions the role of σ_r should not be neglected.

The electron density profile clearly steepens in the plasma edge, but no equivalent feature is seen in the temperature profile, implying the formation of a particle transport barrier only. The increased confinement in the H-mode could be linked to an electron thermal conductivity χ_e which scales as $1/n_e$ and a density rise resulting from the particle barrier.

Particle confinement is thus a central issue in this investigation. Since τ_p^* constitutes the main descriptor, more study is definitely needed to completely characterize τ_p under all conditions. For example, the fact that τ_p^* has no strong species dependence in the cases shown in Table III does not mean that this is also automatically true for τ_p. Other conclusions, however, appear to be more definite. For positive fields at levels below the threshold for the L–H transition an interesting regime is shown to exist; this regime has reduced particle confinement and no noticeable energy confinement loss. Since the edge measurements (such as in Figs 7) yield similar profiles and energies for the exhausted particles in the H_+ and H_- modes, τ_p is also very likely to follow τ_p^* under these circumstances. The particle confinement is typically increased by a factor of about two in H_+ and by a factor of more than four in H_-. Also the energy confinement is increased with either polarity of the applied electric fields. However, the energy confinement in positive H-modes is at least as good as that in negative H-modes.

It is not yet clear how the difference in the improvement can be explained, especially since particle and energy confinement react differently. Several theories [9, 10] attribute the confinement improvement during H-mode conditions to the creation of shear in either the poloidal rotation (dv_θ/dr) or the radial electric field (dE_r/dr). In recent times [20], a consensus appears to develop regarding the predominance of the latter. Both our H_+ modes and the H_- modes have a substantial dE_r/dr of comparable magnitudes and in both cases confinement indeed improves. In Ref. [9] the turbulence quench mechanism is predicted to be insensitive to the sign of either the radial electric field or its shear. On the other hand, Shaing et al. [10] find the best confinement for negative fields and positive field shear. As zones with positive and negative shear are present in both H-modes, a straightforward application of the theory is not possible. The exact location of the zone where this shear is applied may be important. It might also be conceived that actually two effects are superposed: quenching of turbulence by shear, irrespective of the field sign, and a direct sign dependent effect of E_r on transport. The observed asymmetry for fields below the H-mode threshold might be an argument for adding the latter effect; this is also indicated by some neoclassical transport calculations [21, 22].

Combining the energy and particle confinement results, one can conclude that the ratio of τ_p/τ_E is about three times lower in the H_+ mode than in the H_- mode. As mentioned in the introduction, conditions with particle confinement times much higher than the energy confinement time are not desirable in a reactor. In Ref. [4] it was argued that the ratio τ^*_{He}/τ_E should remain below ten to allow ignited, stationary D–T operation. Our present results yield values in excess of what would be tolerable: about 20 in beam heated L-mode discharges, i.e. inside the range $10 \leq \tau^*_{He}/\tau_E \leq 30$ found in an earlier investigation on TEXTOR [23], about 40 in the H_+ conditions and at least 100 in the H_- modes (extrapolating the D_2 and Ne results). The above figures may very well be machine dependent and could be improved by providing a better exhaust efficiency. Given the differences between the H_+ and the H_- conditions, however, it would appear to be of considerable interest to find schemes, other than electrode biasing, to achieve the preferential electron loss from the plasma that is necessary for setting up positive H-modes.

Appendix A
RECYCLING AND EXHAUST MODELLING

The decay times τ^*_p and the partial pressure in the pumping duct depend in a rather intricate way on the particle confinement time of the respective ions. In order to derive the latter, a recycling model has to be considered which incorporates the most important physical effects, such as those proposed in Ref. [18] and extended hereafter to include pumping. Particles of a given species are injected through a gas feed in the torus at a rate Q. At later times, they can be retrieved in one of four reservoirs: the plasma (total number at a given time = N_p, all being ions), the SOL (total number N_B, all neutrals), the wall (total number N_w) and the pumps (total number of particles pumped N_E). The first three reservoirs can hold the atoms (ions) during their respective 'confinement times' τ_p, τ_B and τ_w. The fuelling efficiency f takes into account that some of the neutrals leaving the limiting surfaces are ionized in the SOL such that they will be convected as ions to the limiter instead of fuelling the plasma. The reflection coefficient R is equal to the probability of a particle incident on the wall to be reflected. Note that most of the wall implanted trace elements will leave the wall under bombardment by the deuterium flux. This effect is incorporated in τ_w.

The N_E particles that are potentially pumped are ions that reside on field lines meeting the pump duct openings of ALT-II. There are two types of these: (i) ions that leave the plasma at a rate N_p/τ_p, a fraction ϵ_1 of which is exhausted; and (ii) refuelling neutrals $(1 - f)\,N_B/\tau_B$ that happen to be reionized in the SOL and are removed with efficiency ϵ_2. The fraction ϵ_i should also take into account that some of the incident particles will be returned via backscattering to the plasma after neutralization on the deflector plates. Quite often, no distinction is made between these two categories [23], and the global exhaust efficiency ϵ is defined in terms of N_p/τ_p only. A typical figure is 0.08–0.10 for deuterium and helium, using the full pumping capability of ALT-II [23]. It is easy to show in the context of our model that this approximation is warranted when

$$(1 - f)\,\epsilon_2 < f\epsilon_1 \qquad (A.1)$$

i.e. when f is sufficiently close to unity, and then leads to $\epsilon = \epsilon_1$. An approximate evaluation of ϵ_i is given in Appendix B.

The four equations describing the time evolution of N_p, N_B, N_w and N_E are:

$$\frac{dN_p}{dt} = -\frac{N_p}{\tau_p} + f\frac{N_B}{\tau_B} \qquad (A.2)$$

$$\frac{dN_B}{dt} = -\frac{N_B}{\tau_B} + \frac{N_w}{\tau_w} + R(1-\epsilon_1)\frac{N_p}{\tau_p} + Q \quad (A.3)$$

$$\frac{dN_w}{dt} = -\frac{N_w}{\tau_w} + (1-\epsilon_2)(1-f)\frac{N_B}{\tau_B} + (1-R)(1-\epsilon_1)\frac{N_p}{\tau_p} \quad (A.4)$$

$$\frac{dN_E}{dt} = \epsilon_1\frac{N_p}{\tau_p} + \epsilon_2(1-f)\frac{N_B}{\tau_B} \quad (A.5)$$

It can be verified that this system conserves the total number of injected particles $N_{tot} = N_p + N_B + N_w + N_E = \int Q dt$.

The time τ_B is very small, since it roughly corresponds to the transit time of a wall released neutral through the SOL. Except for a short transient after any perturbation, N_B can therefore be treated as stationary. Assuming furthermore that Eq. (A.1) prevails and that the gas injection is stopped ($Q = 0$), the following analytic results can be obtained from this model:

Equations (A.2) to (A.5) reduce to the simpler set

$$\frac{dN_p}{dt} + (1+a\epsilon)\frac{N_p}{\tau_p'} - \frac{N_w}{\tau_w'} = 0 \quad (A.6)$$

$$\frac{dN_w}{dt} - (1-\epsilon)\frac{N_p}{\tau_p'} + \frac{N_w}{\tau_w'} = 0 \quad (A.7)$$

where

$$\tau_p' = \frac{\tau_p}{1-fR}, \quad \tau_w' = \frac{\tau_w}{f} \text{ and } a = \frac{fR}{1-fR}$$

The solutions are of the form

$$N_p(t) = C_1 \exp(-t/\tau_1) + C_2 \exp(-t/\tau_2) \quad (A.8)$$

where $\tau_{1,2}$ are given by

$$\frac{2}{\tau_{1,2}} = \left[\left(\frac{1}{\tau_p'} + \frac{1}{\tau_w'}\right) + \epsilon\frac{a}{\tau_p'}\right] \pm \sqrt{\left[\left(\frac{1}{\tau_p'} + \frac{1}{\tau_w'}\right) + \epsilon\frac{a}{\tau_p'}\right]^2 - \frac{4\epsilon}{(1-fR)\tau_p'\tau_w'}} \quad (A.9)$$

(a) Without pumping ($\epsilon = 0$), the solutions of Eq. (A.9) are

$$\tau_1 = \frac{\tau_p'\tau_w'}{\tau_w' + \tau_p'} \quad \text{and} \quad \tau_2 = \infty$$

yielding a fast decay to a stationary level of N_p ($N_{p,s}$) (case Fig. 12(b)) which is found to be given by

$$N_{p,s} = \frac{f\tau_p}{(1-fR)\tau_w + f\tau_p} N_{tot} \quad (A.10)$$

The fact that this level is attained after an overshoot could be explained by the reservoir action of the wall.

(b) When $\epsilon \neq 0$ but $\ll 1$ (typically of order 0.1 in the experiment), the fast time constant τ_1 remains practically unchanged, but τ_2 is no longer infinite (situation of Fig. 12(a)). As long as

$$\frac{4\epsilon}{(1-fR)\tau_p'\tau_w'} \ll \left[\left(\frac{1}{\tau_p'} + \frac{1}{\tau_w'}\right) + \epsilon\frac{a}{\tau_p'}\right]^2, \quad \text{i.e. } \epsilon \ll 1,$$

an approximate solution of Eq. (A.9) is

$$\frac{1}{\tau_2} = \frac{\epsilon}{\dfrac{(1-fR)\tau_p'\tau_w'}{\dfrac{1}{\tau_p'} + \dfrac{1}{\tau_w'} + \epsilon\dfrac{a}{\tau_p'}}}$$

In the same approximation, τ_2 (henceforth called τ_p^*, the decay rate resulting from pumping) can finally be written as

$$\tau_p^* = ((1-fR)\tau_w + f\tau_p)/f\epsilon \quad (A.11)$$

(c) The partial pressure measured in the duct is given by

$$p = 4.4 \times 10^{-21} N_{tot}/(\tau_p^* S_{eff}) \quad (A.12)$$

where S_{eff} is the effective pumping speed for the species considered. A temperature of 300 K in the pump volume is assumed, and SI units are used.

Appendix B

EXHAUST AND FUELLING EFFICIENCY AS A FUNCTION OF CHANGES IN THE SOL

(1) Exhaust efficiency

The exhaust efficiency ($\epsilon = \epsilon_1$) as defined in Appendix A is given by the ratio of the flow effectively removed by the pump limiter to the total efflux, N_p/τ_p, of ions of a given species from the plasma. In Ref. [23], almost identical values of ϵ were found for deuterium and helium. Here, we will assume that the efficiency is the same for all species. As shown in Ref. [24], the particle removal can be divided into two separate stages. The first stage requires collecting plasma in the scoops under the pump limiter blades. The efficiency with which the limiter is capable of capturing

the charged particle flow from the core into the scoops is called the collection efficiency, η = scoop flux/core efflux. The second stage involves the efficiency with which the neutrals that result from the neutralization of the impinging ions on the neutralization plates are removed by the pumps. This efficiency is called the removal efficiency and is given by ζ = pumped flux/scoop flux. Finally,

$$\epsilon = \eta \zeta$$

Since the flux $\Gamma_{\parallel}(r)$ that impinges on the limiter along the magnetic field lines is given by $n(r)\, v_{\parallel}(r)$, where $v_{\parallel} \approx 0.3\, C_s \approx 0.3 \sqrt{(KT_e/m_i)}$, η can be written as

$$\eta = \frac{\int_{r_2}^{r_1} n \sqrt{T_e}\, dr}{\int_{r_w}^{r_L} n \sqrt{T_e}\, dr} \qquad \text{(B.1)}$$

where the integration boundaries are given by the radii of the scoop aperture (r_1 = 47.7 cm and r_2 = 50.2 cm) and of the SOL boundaries (r_L = 46.0 cm and r_w = 55 cm). In the case where, unlike in our experiments, n and T have an exponential r-dependence, with respective scale lengths λ_n and λ_T, Eq. (B.1) reduces to

$$\eta = (1 - \exp(-(r_1 - r_L)/\lambda_\Gamma) \exp(-(r_2 - r_1)/\lambda_\Gamma)$$

where $\lambda_\Gamma = (2\lambda_n\lambda_T)/(\lambda_n + 2\lambda_T)$, and where it is also assumed that $r_w - r_L$ is much larger than λ_Γ.

Equation (B.1) yields the experimental dependence of η on V_E shown in Fig. 21. A reduction of the collection efficiency to about two thirds of its no-bias value can be expected under H-mode conditions.

The removal efficiency ζ can be written as

$$\zeta = \frac{S_{eff}}{S_{eff} + C}$$

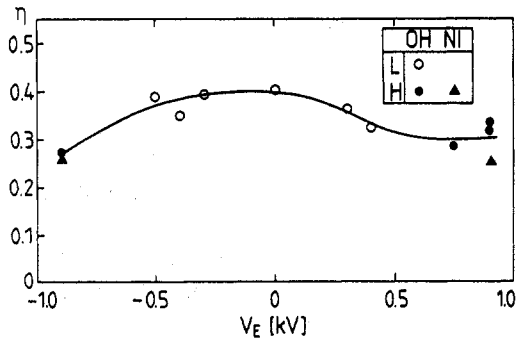

FIG. 21. Variation of the computed collection efficiency η of the pump limiter with the electrode voltage V_E for different conditions identified in the inset.

TABLE V. FUELLING EFFICIENCY FOR RECYCLING D, He AND Ne ATOMS

V_E (V)	f		
	D	He	Ne
-300	0.78	0.90	0.68
0	0.78	0.88	0.60
+300	0.96	0.98	0.94
+900	0.97	0.98	0.93

where S_{eff} is the effective pumping speed of the vacuum pumps for the given species and C is the effective particle backflow conductance through the scoops into the vessel. This parameter is difficult to quantify and could be quite different for different species. The backflow conductance has been studied in Ref. [16] for deuterium and helium species and was shown to decrease with increasing incident particle flow, the effect being more pronounced for helium than for deuterium. Figure 9 shows the variation of density in front of the pump duct openings. Since the electron temperature is almost constant for the conditions shown (T_e = 20 ± 4 eV), the impinging flow at V_E = 300 and 750 V decreases by a factor of four with respect to the no-bias condition. Such changes lead in the investigation of Ref. [16] under all conditions studied to variations in C between 1.2 and 2. Since a typical value for the removal efficiency is 0.3 [24, 25], the expected decrease of ζ with respect to the no-bias case ranges between 1.15 and 1.6.

Combining the variation of η and ζ, we conclude that the dependence of ϵ on V_E will be stronger than that shown in Fig. 21. For the conditions of Table I, we estimate a relative change in ϵ with respect to V_E = 0 of 0.70 at V_E = 300 V and of 0.55 at V_E = 750 V.

As a general conclusion, one should note that reductions by a factor of two in ϵ could be expected under some H-mode conditions. More work on this subject is, however, certainly needed.

(2) Fuelling efficiency

The fraction of neutral atoms, launched at a radius r_b with velocity v_b, that reach the limiter radius r_L without being ionized can be expressed as

$$f = \exp\left(-\int_{r_L}^{r_b} \frac{n_e \langle \sigma v_e \rangle}{v_b}\, dr\right) \qquad \text{(B.2)}$$

where n_e is the electron density and $\langle \sigma v_e \rangle$ is the ionization rate. Using the experimental n_e and T_e profiles,

Eq. (B.2) has been evaluated for thermal D, He and Ne atoms (for a mean thermal velocity v_b corresponding to 450 K, thus neglecting a possible energy dependence of f), assuming the ionization rates by electron collisions given in Ref. [26]. If the radius of birth r_b is chosen to be equal to $r_L + \Delta_n$, where Δ_n is the average depth to which the outflowing ions penetrate into the SOL before being convected to the limiter or wall (taken here as the distance over which n_e drops to 1/e of its value at the limiter radius), Eq. (B.2) is thought to be a first, rough approximation of the fuelling efficiency, since, for example, ionization from excited states after collisional excitation is ignored. Table V lists, for four typical Ohmic conditions, the results thus obtained for the three species. In the case of neon, significant changes in fuelling efficiency can be expected between the conditions at $V_E = 0$ V and those at $V_E = 350$ and 900 V.

REFERENCES

[1] WAGNER, F., BECKER, G., BEHRINGER, K., Phys. Rev. Lett. **49** (1982) 1408.

[2] SIPS, A.C.C., DE HAAS, J.C.M., HOGEWEY, G.M.D., et al., Bull. Am. Phys. Soc. **34** (1989) 2055.

[3] BECKER, G., Nucl. Fusion **28** (1988) 1458.

[4] REITER, D., WOLF, G.H., KEVER, H., Nucl. Fusion **30** (1990) 2141.

[5] TAYLOR, R.J., BROWN, M.L., FRIED, B.D., et al., Phys. Rev. Lett. **63** (1989) 2365.

[6] WEYNANTS, R.R., TAYLOR, R.J., VANDENPLAS, P.E., et al., in Controlled Fusion and Plasma Heating (Proc. 17th Eur. Conf. Amsterdam, 1990), Vol. 14B, Part I, European Physical Society (1990) 287.

[7] WEYNANTS, R.R., BORA, D., DELVIGNE, T., et al., in Plasma Physics and Controlled Nuclear Fusion Research 1990 (Proc. 13th Int. Conf. Washington, DC, 1990), Vol. 1, IAEA, Vienna (1991) 473.

[8] GROEBNER, R.J., BURRELL, K.H., SERAYDARIAN, R.P., Phys. Rev. Lett. **64** (1990) 3015.

[9] BIGLARI, H., DIAMOND, P.H., TERRY, P.W., Phys. Fluids B **2** (1990) 1.

[10] SHAING, K.C., CRUME, E.C., Jr., HOULBERG, W.A., Phys. Fluids B **2** (1990) 1492.

[11] KIM, Y.B., DIAMOND, P.H., BIGLARI, H., CALLEN, J.D., Phys. Fluids B **3** (1991) 384.

[12] VAN NIEUWENHOVE, R., VAN OOST, G., WEYNANTS, R.R., et al., in Controlled Fusion and Plasma Physics (Proc. 18th Eur. Conf. Berlin, 1991), Vol. 15C, Part I, European Physical Society (1991) 405.

[13] WEYNANTS, R.R., TAYLOR, R.J., Nucl. Fusion **30** (1990) 945.

[14] SHAING, K.C., CRUME, E.C., Jr., Phys. Rev. Lett. **63** (1989) 2369.

[15] HILLIS, D.L., WEYNANTS, R.R., HOGAN, J.T., et al., Helium exhaust and transport studies of enhanced confinement plasmas induced by edge polarization in the TEXTOR tokamak, to be submitted for publication.

[16] HARDTKE, H., DIPPEL, K.-H., FINKEN, K.-H., et al., J. Nucl. Mater. **162–164** (1989) 661.

[17] JOHNSON, L.C., HINNOV, E., J. Quant. Spectrosc. Radiat. Transfer **13** (1973) 333.

[18] EHRENBERG, J., COAD, P., DE KOCK, L., et al., J. Nucl. Mater. **162–164** (1989) 63.

[19] CALLEN, J.D., CHRISTIANSEN, J.P., CORDEY, J.G., et al., Nucl. Fusion **27** (1987) 1857.

[20] BIGLARI, H., in 3rd Workshop on H-mode Physics, Vol. 2, JET Joint Undertaking, Abingdon, Oxfordshire (1991) 539, and other papers.

[21] CONNOR, J.W., Plasma Phys. **15** (1973) 765.

[22] STRINGER, T.E., Neoclassical transport in the presence of fluctuations, submitted to Nucl. Fusion.

[23] HILLIS, D.L., FINKEN, K.-H., HOGAN, J.T., et al., Phys. Rev. Lett. **65** (1990) 2382.

[24] CORBETT, J., Tokamak Experiments with a Toroidal Pump Limiter, PhD Thesis, Mechanical, Aerospace and Engineering Department, University of California, Los Angeles (1989).

[25] DIPPEL, K.-H., FINKEN, K.-H., HARDTKE, A., et al., in Plasma Physics and Controlled Nuclear Fusion Research 1988 (Proc. 12th Int. Conf. Nice, 1988), Vol. 1, IAEA, Vienna (1989) 453.

[26] ARNAUD, M., ROTHENFLUG, R., Astron. Astrophys. Supp. Ser. **60** (1985) 425.

(Manuscript received 23 September 1991
Final manuscript received 3 February 1992)